© creative

Scientific paper

Synthesis, Spectroscopy, X-ray Structures, DNA Binding and Photocatalytic Properties of Two Ni(II) and Co(II) Complexes of a Pyrazolyl Schiff-base Ligand

Suman Mandal,¹ David B. Cordes,² Alexandra M. Z. Slawin² and Nitis Chandra Saha (1)^{1,*}

¹ Department of Chemistry, University of Kalyani, Nadia, West Bengal-741235, India

² School of Chemistry, University of St Andrews, North Haugh, St Andrews, Fife KY16 9ST, UK

* Corresponding author: E-mail: nitissaha@klyuniv.ac.in Phone: +91-33-2582-8750 (Extn: 309)

Received: 08-13-2023

Abstract

Two new nickel(II) and cobalt(II) complexes, $[Ni(MPAFA)_3](BF_4)_2$ (I) and $[Co(MPAFA)_3](BF_4)_2$ (II) were synthesized from a pyrazole containing 'NN' bidentate Schiff-base ligand, N-(furan-2-ylmethyl)-1-(5-methyl-1H-pyrazol-3-yl)methanimine, (MPAFA) (L). The complexes I and II were characterized by various physico-chemical and spectral parameters. Both I and II were 1:3 (M:L) coordination complexes and behaving as 1:2 electrolytes. Single crystal X-ray diffraction studies revealed that both of them were distorted octahedral in nature with a N6 donor set. The binding interactions of the complexes with CT-DNA were studied by UV-Vis and fluorescence spectroscopic methods. I was found to bind with CT-DNA in a partial intercalative mode, whereas II bound via the groove-like manner in solutions. The ligand and the complexes were shown to have potential photocatalytic activity in degrading methylene-blue (MB) under UV-Vis light irradiation.

Keywords: Pyrazole, Schiff-base ligand, Ni(II) and Co(II) complexes, X-ray structures, CT-DNA, Photocatalytic activity.

1. Introduction

The amazing biological capabilities of Schiff bases and their transition metal complexes, as well as their extensive applicability in other domains such as pigments and dyes, catalyst carriers, corrosion inhibitors, polymer stabilizers and thermos-stable substances etc., attracted a lot of attention to their chemistry. 1-3 Normally Schiff base ligands and their metal ion complexes exhibit a wide range of significant biological activities and also possess many important therapeutic applications in a variety of fields, including antibacterial, anticancer, antifungal, anti-malarial, antiproliferative, antiviral, antipyretic and anti-inflammatory activities.4-7 Transition metal complexes of Schiff base ligands belong to an important class that plays a key role in biology because of their unique photochemical or electrochemical properties, well-defined coordination patterns, and tendency to interact with DNA.8,9 Due to their ease in forming stable complexes with the majority of transition metals, Schiff bases play a significant role in inor-

ganic chemistry also. 10 Recent years have witnessed a tremendous development in interactions between metal ions and nucleic acids, which has created a challenging research area in inorganic and structural chemistry. 11 In coordination chemistry, considering the synthetic work, catalytic activity, bioactivity and physico-chemical study, N and O donor Schiff base ligands with their metal complexes have long been crucial. 12,13 The wide-ranging pharmacophoric characteristics of such Schiff bases are in the creation of a variety of top biologically active compounds. 14 The metal complexes of these ligands have the potential to bind DNA molecules precisely and be developed as pharmaceuticals. Several scientists have shown their keen interest in metal-containing medications and their modes of interaction with proteins and DNA. 15-17 The fundamental mechanism for the cytotoxic activities of some metal-based medications is assumed to be ROS generation and subsequent destruction of the DNA helix and/ or mitochondrial membrane potential, leading to the induction of apoptosis. In

order to produce more potent medications that would target DNA, the association of bioinorganic compounds with DNA has drawn increased interest.^{18,19}

It is known that human physiology depends largely on a number of trace elements like Ni, Co, Zn etc.^{20,21} The biological significance of nickel is gradually becoming understood.^{22,23} Nickel complexes of the Schiff base ligands have displayed impressive antioxidant,²⁴ antifungal,²⁵ anticancer,²⁶ antibacterial²⁷ and antiproliferative²⁸ activities in the hunt for new metal-based medications. Cobalt plays a decisive role in numerous biologically important processes in human body, and majority of it is present in the form of vitamin B12 (cobalamin).²⁹ Because of their powerful antibacterial, antiviral, antifungal, antiprotozoal and anticancer properties, Schiff base complexes with cobalt have drawn much interest for their interactions with biomolecules such as proteins and nucleic acids, and a large number of therapeutically relevant cobalt complexes have been prepared.^{30–34}

In the present days organic dyes, one of the main pollutants in wastewater, have received a great deal of attention due to their reduction in water quality and harmful effects on aquatic creatures as well as on human health.^{35,36} Degradation/ destruction of various organic dyes represents a big challenge to human civilization, and coordination compounds have recently gained a lot of attention for the investigation of photocatalytic degradation of such organic dyes in water. 37-43 Coordination polymers (Cps) obtained from reactions between Schiff bases and transition metals, are now being used as catalysts in photocatalytic dye degradation, which is decisive for industrial waste water treatment. There have been considerable efforts in the treatment of industrial wastewater based on adsorption and separation, 44,45 chemical treatment 46 and photocatalytic methods.⁴⁷ Among them, photocatalysis is a practical, economical and reliable method that has been used to remove toxins like organic dyes safely and effectively from the environment. 48-51 Schiff base coordinated Ni(II) and Co(II) complexes show promising photocatalytic activities for the degradation of organic dyes.⁵²⁻⁵⁴

In this submission, we have described the synthesis, characterization, spectroscopy and structural elucidation of two new Ni(II) and Co(II) complexes, [Ni(MPAFA)₃] (BF₄)₂ (I) and [Co(MPAFA)₃](BF₄)₂ (II) of a 'NN' bidentate Schiff base ligand, N-(furan-2-ylmethyl)-1-(5-methyl-1H-pyrazol-3-yl)methanimine, (MPAFA). DNA binding interaction of the complexes with CT-DNA and photocatalytic degradation of methylene blue (MB) dye by the ligand and the complexes have also been reported here.

2. Experimental

All reagents were of AR/GR grade and obtained from commercial sources and used without further purification. The metal salts and other organic chemicals and solvents were purchased from SIGMA ALDRICH CHEMICALS

PVT. LTD. For conductance and spectral measurements, Spectro-grade methanol purchased from SPECTRO-CHEM was used.

2. 1. Synthesis of the Ni(II) and Co(II) Complexes: [Ni(MPAFA)₃](BF₄)₂ (I) and [Co(MPAFA)₃](BF₄)₂ (II)

The Ni(II) and Co(II) complexes were synthesized by refluxing a 3:1 molar mixture of the ligand⁵⁵ (0.3968 gm, 0.0021 mol) and Ni(BF₄)₂.6H₂O (for I) and Co(B- F_4 ₂.6 H_2 O (for II) salts (0.0007 mol each) in ethanol for about an hour on a boiling water bath. On slow evaporation of the resulting greenish vellow / reddish solutions, the desired Ni(II) and Co(II) complexes crystallized, they were filtered off, washed with ethanol, dried over anhydrous CaCl₂ (yield ~ 76-80%). X-ray quality single crystals of [Ni(MPAFA)₃](BF₄)₂ (I) and [Co(MPAFA)₃](BF₄)₂ (II) were obtained from chloroform-n hexane mixture by solvent diffusion technique. Anal. Calcd. (%) for C₃₀H₃₃B-₂F₈N₉NiO₃ (**I**): C, 45.2; H, 4.3; N, 15.8; Ni, 7.5. Found (%): C, 45.0; H, 4.1; N, 15.7; Ni, 7.3. $\Lambda_{\rm m}$ (MeOH): 196 Ω^{-1} cm² mol⁻¹ at 30 °C. μ_{eff} 3.01 BM at 300 K. IR (KBr) ν (cm⁻¹): 1634 ($\nu_{CH=N,\,azomethine}$), 1577 ($\nu_{C=N,\,pyrazole}$), 1049 ($\nu_{N-N,\,pyrazole}$) and 476 ($\nu_{Ni-N,\,azomethine}$). UV-Vis. (MeOH, λ_{max} , nm): $217 (\pi \rightarrow \pi^*)$, $239 (n \rightarrow \pi^*)$, $552 (d \rightarrow d)$.

Anal. Calcd. (%) for $C_{30}H_{33}B_2F_8N_9CoO_3$ (II): C, 45.2; H, 4.2; N, 15.9; Co, 7.6. Found (%): C, 45.1; H, 4.0; N, 15.6; Co, 7.4. Λ_m (MeOH): $101~\Omega^{-1}~cm^2~mol^{-1}$ at 30 °C. μ_{eff} 1.98 BM at 300 K. IR (KBr) ν (cm⁻¹): 1634 (ν_{CH=N, azomethine}), 1576 (ν_{C=N, pyrazole}), 1081 (ν_{N-N, pyrazole}) and 459 (ν_{Co-N, azomethine}). UV-Vis. (MeOH, λ_{max} , nm): 218 (π \rightarrow π*), 240 (n \rightarrow π*), 585 (d \rightarrow d).

2. 2. Physical Measurements

The molar conductance values of the complexes in methanol were measured using a Systronics 308 digital conductivity metre. A Perkin-Elmer 2400 CHNS/O analyser was employed to carry out the elemental analyses (C, H, and N). The nickel and cobalt contents of the complexes were determined gravimetrically as dimethylglyoximatonickel(II) and anhydrous CoSO₄, respectively. Using KBr pellets, IR spectra (4000–450 cm⁻¹) of the complexes were measured on a Perkin Elmer Model Spectrum Two FT-IR spectrophotometer. Magnetic susceptibilities were measured in the polycrystalline state on a PAR 155 sample vibrating magnetometer. The UV-Vis spectral study was performed on a Shimadzu UV-1900i spectrophotometer in MeOH. The fluorescence spectra of the complexes in methanol were recorded using a Hitachi F-7100 Fluorescence Spectrometer. A Shimadzu UV-1900i spectrophotometer was used to study the photocatalytic degradation of Methylene Blue (MB) and a UV-400 type photochemical reactor equipped with 400 W mercury lamp was used as the UV and Visible light source during the irradiation process.

2. 3. Crystallographic Measurements

Diffraction data for complexes I and II were collected at 173 K using a Rigaku FR-X Ultrahigh Brilliance Microfocus RA generator/confocal optics with XtaLAB P200 diffractometer [Mo K α radiation ($\lambda = 0.71073 \text{ Å}$)]. All intensity data were collected at 173 K, using either both ω and φ steps or just ω steps, accumulating area detector images spanning at least a hemisphere of reciprocal space. Data were collected using CrystalClear⁵⁶ and processed (including correction for Lorentz, polarization and absorption) using CrysAlisPro.⁵⁷ Structures were solved by dual-space (SHELXT)⁵⁸ or direct (SIR2004)⁵⁹ methods and refined by full-matrix least-squares against F² (SHELXL-2018/3).⁶⁰ Non-hydrogen atoms were refined anisotropically, and carbon-bound hydrogen atoms were refined using a riding model. Hydrogen atoms bound to heteroatoms were located from the difference Fourier map and refined isotropically subject to a distance restraint. The structures of both complexes showed disorder in their anions, these were modelled over two sites with occupancies of 0.91:0.09 and 0.79:0.21 for I and 0.88:0.12 and 0.78:0.22 for II. Fluorine atoms in the minor component of the disorder were refined isotropically, and restraints to bond distances and thermal motion were used. All calculations were performed using the Olex261 interface.

2. 4. DNA binding Studies

2. 4. 1. Absorption Spectral Studies

UV-Vis titration of a tris-HCl buffer (30 mM) at pH 7.5 at room temperature was used to assess the DNA binding characteristics of complexes I and II. The titration experiment was carried out in a quartz cuvette holding a constant concentration of each complex $(1.25 \times 10^{-4} \text{ M})$ and a changing concentration of CT-DNA (0–5.769 \times 10⁻⁵ M). The concentration of the CT-DNA solution was determined by absorption spectroscopy using 13,600 M⁻¹ cm⁻¹ molar extinction coefficient at 260 nm. 62 To eliminate the DNA's particular absorbance, equal quantities of CT-DNA solution were added to the complex and standard solutions. Each complex received a DNA addition in Tris-HCl buffer, and the resultant solution was allowed to reach equilibrium at 25 °C for 10 minutes. The absorbances for I and II were calculated while being scanned at 240 and 244 nm, respectively.

2. 4. 2. Emission Spectral Studies

The fluorescence displacement assays with ethidium bromide (EB) were performed at 25 °C in a 30 mM Tris-HCl buffer (pH 7.5). First, the CT-DNA was incubated in a darkened atmosphere for around 30 minutes at 35 °C with ethidium bromide ([EB]/[DNA] = 0.1).⁶³ The resultant complex was then adjusted from $0-6.725 \times 10^{-3}$ M in an EB-bound CT-DNA solution. The effects of flu-

orescence quenching were determined by observing how the spectrum of fluorescence emission changed at varying concentrations of complexes. After excitation of the sample solutions at 510 nm, the fluorescence intensities for I and II were measured at 591 nm and 590 nm, respectively.

2. 4. 3. Viscosity Measurement

A thermostatic water bath was used to evaluate the viscosity in a buffer containing 30 mM Tris-HCl at a constant temperature of 25 °C (pH 7.5). The plots of binding ratio ([complex]/[DNA]) vs. relative specific viscosity $\{(\eta/\eta_0)^{1/3}\}$ were obtained for **I** and **II**, where [complex]/[DNA] = 0, 0.2, 0.6, 1.0, 1.4, 2.0; η and η_0 were the specific viscosities of CT-DNA in the presence and in absence of the complexes, respectively. The equation $\eta = (t-t_0)/t_0$ was used to calculate the relative viscosity, where t was the flow time of the CT-DNA solution in the absence or presence of the complex and t_0 represented the flow time of the Tris-HCl buffer solution. CT-DNA was present at a concentration of 25×10^{-5} M. The flow time of each sample was measured three times with a digital stopwatch, and the average flow time was calculated.

2. 5. Photocatalytic Experiment

Methylene Blue (MB) was used as the target dye in the investigation of photocatalytic activity of the ligand (L) and its complexes (I and II). Each compound could be well dispersed in the dye solution prior to the photocatalytic degradation experiment. 0.015 mmol of solid compound was added into 100 mL of MB aqueous solution (10 mg/L). The compounds were magnetically stirred for 30 minutes in the dark until an adsorption-desorption equilibrium was reached before applying UV radiation. The mixture was then exposed to UV and visible light for 140 minutes. Samples were taken every 20 minutes interval throughout this time, and their absorbances were continually measured. To determine the photosensitivity of MB, the same experimental setup was used for the blank experiment (without the addition of compounds). The following equation was used to compute the degradation efficiencies of photocatalysts:

 $D\% = A_t/A_0 x100\%$

D% = the degradation efficiencies of photocatalysts.

 A_0 = the initial absorbance values of the MB aqueous solution.

 A_t = the absorbance values of the MB aqueous solution at time t.

3. Results and Discussion

3. 1. Synthesis and Characterization

The two new mononuclear complexes, $[M^{II}(MPA-FA)_3](BF_4)_2$ (where, M = Ni and Co for I and II, respec-

tively) were prepared by refluxing ethanol solution of three equivalent of the ligand, MPAFA and one equivalent of respective metal tetrafluoroborate salt in each case (Scheme 1). Elemental analyses of the complexes were in good agreement with the molecular structures determined by the single crystal X-ray studies.

measured in methanol. The electronic spectrum of the free ligand exhibited a band at 368 nm, assigned to the $(n\rightarrow\pi^*)$ transition of the azomethine group. A noticeable band observed at 235 nm, which might be a $(\pi\rightarrow\pi^*)$ transition.⁶⁵ The ligand to metal charge transfer (LMCT) bands for the Ni(II) and Co(II) complexes were visible at 217–218 and

Scheme 1. Synthetic procedure of the complexes I and II.

3. 2. IR spectra

Upon comparison of the infrared bands (4000-450 cm⁻¹) of the complexes with those of the free ligand, valuable information on the bonding sites of the primary ligand molecule was obtained. A negative shift in $\nu_{(CH=N, azomethine)}$ (1650 cm⁻¹) band in the spectrum of the free ligand to lower values1633-1634 cm⁻¹ in the complexes was consistent with the coordination of the azomethine nitrogen to the central metal ion. The pyrazolyl tertiary ring nitrogen atom (2N) as a potential binding site was indicated by the shifting of the $\nu_{(C=N,\;pyrazole\;ring)}$ bands of the complexes to a higher frequency range 1576-1581 cm⁻¹ than the free ligand itself at 1540 cm⁻¹. A relatively strong IR band at 1010 cm⁻¹ in the free ligand, due to $v_{(N-N, pvrazole)}$ vibration, was also found to shift to the higher wave numbers 1049-1081 cm⁻¹ in the metal complexes. This offered additional evidence that the tertiary nitrogen (2N) atom of pyrazole ring participated in bonding.64 The appearance of new IR bands at 459-481 cm⁻¹ in the spectra of the complexes were then assigned to $v_{(M-N)}$ vibrations (Figures S1 and S2).

3. 3. UV-Vis Spectra

The electronic absorption spectra of the free Schiff base ligand and its Ni(II) and Co(II) complexes were

239–240 nm for $(\pi \rightarrow \pi^*)$ and $(n \rightarrow \pi^*)$ transitions, respectively, as well as a low intensity major band for the d–d transition of a metal ion at 552–585 nm was also observed⁶⁶ (Figures S3 and S4).

3. 4. Fluorescence Property

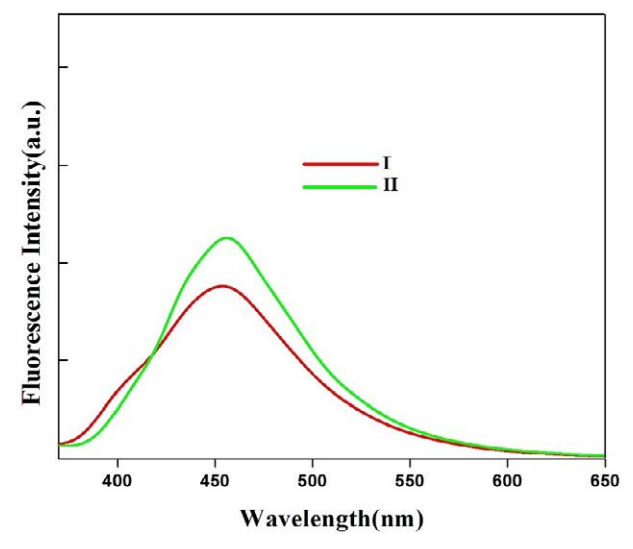


Figure 1. Fluorescence spectra of the complexes in I and II in MeOH

The fluorescence spectra of the complexes were recorded in methanol at a concentration of 2×10^{-5} M. The complex species displayed distinctive fluorescence traits. When the complexes were stimulated at wavelengths between 247 and 239 nm, the emission bands were found to be discernible between 453 and 456 nm (Table S1, Figure 1). Among the complexes, II was more fluorescent than I. It demonstrated a strong emission band at the highest emission wavelength of 456 nm at the excitation wave length of 239 nm. The probable causes for the emission phenomenon displayed by the complexes might be due to the ligand to metal charge transfer (LMCT). The data suggested that both I and II in particular, might be the suitable candidate for a photoactive molecule.

3. 5. Structural Description

ORTEP-3⁶⁷ plots of the complexes, [Ni(MPAFA)₃] $(BF_4)_2$ (I) and $[Co(MPAFA)_3](BF_4)_2$ (II) together with the atom numbering schemes are shown in Figures 2 and 3, respectively. The crystallographic data and refinement parameters are summarized in Table 1. The asymmetric unit of each structure consists of a [M(MPAFA)₃]²⁺ cation, and two BF₄⁻ counter ions, and complexes I and II are isostructural to the related complex [Ni(MPAFA)₃](ClO₄)₂ 55 The two complex cations reported here and the isostructural complex⁵⁵ are geometrically very similar; selected bond distances and bond angles in the structures of I, II and [Ni(MPAFA)₃](ClO₄)₂ are compiled in Table 2. Like the isostructural complex,⁵⁵ the metal centres, in both the complexes I and II, display a distorted octahedral geometry and three neutral MPAFA molecules upon coordination to the respective metal centres, generate a N6 donor set. Each bidentate ligand molecule bonded to the metal ion via the azomethine and the pyrazolyl (tertiary) nitrogen atoms; two of the pyrazolyl nitrogen atoms (N16 and N30 for I;

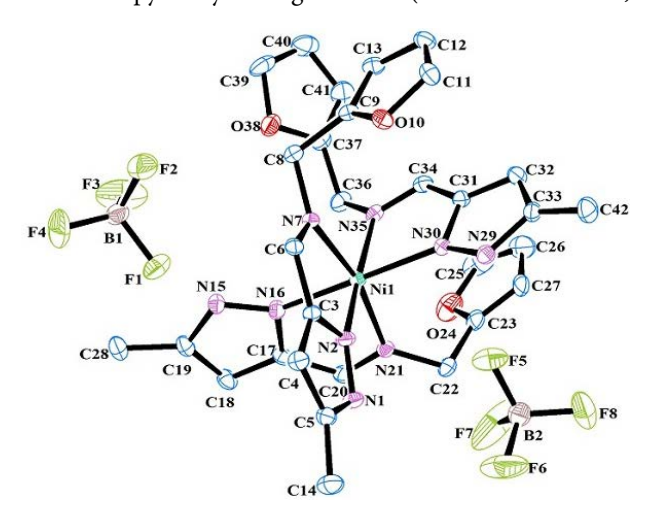


Figure 2. Ortep-3 diagram (30% probability ellipsoids) of complex I with atom numbering scheme (hydrogen atoms are omitted for clarity).

N2 and N30 for **II**), two of the azomethine nitrogen atoms (N7 and N35 for **I**; N7 and N21 for **II**) and the remaining pyrazolyl nitrogen and the azomethine nitrogen atoms (N2 and N21 for **I**; N16 and N35 for **II**) coordinate to Ni1/ Co1 in a *trans*, *cis* and *cis* manner, respectively.

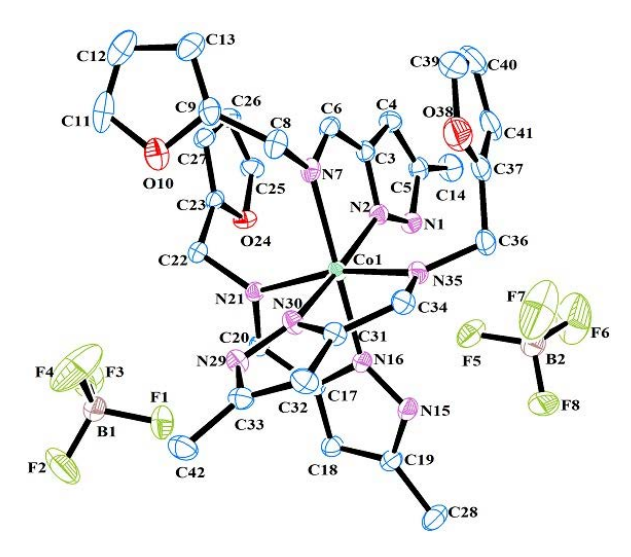


Figure 3. Ortep-3 diagram (30% probability ellipsoids) of complex II with atom numbering scheme (hydrogen atoms are omitted for clarity)

Strong N-H...F hydrogen bonding interactions are observed in the crystal lattices of both I and II. The tetrafluoroborate anions and the pyrazolyl N-H groups play significant role in the formation of H-bonding interactions as shown in Figures 4 and 5. The details of the hydrogen bonding interactions observed in I and II are summarized in Table 3. $\pi \cdot \cdot \cdot \pi$ stacking interactions have also been identified in both the complex species. In I, intramolecular offset π···π stacking interaction is observed between the pyrazole ring (N29-N30-C31-C32-C33) of one ligand and the furan ring (C9-O10-C11-C12-C13) of another ligand; while in II, the same is observed between the rings (N1-N2-C3-C4-C5) and (C23-O24-C25-C26-C27). The distances between the centroids of pyrazole and furan rings involved in the stacking interactions are 3.658 and 3.650 Å, and angles between the mean planes of the rings are 7.81 and 7.02°, and the offset between the centroids (in the plane of one ring) are 0.98 and 0.88 Å for I and II, respectively (Figures 4 and 5). The stacking interactions, in both the complex species, are quite strong,68,69 given the offset as well as the relatively short distance between centroids, making the complex molecules more stable. Crystal packing of I and II are shown in Figures S5 and S6, respectively.

3. 6. DNA binding Performance

3. 6. 1. Stability of the Complexes

In research on biological activity, dimethyl sulphoxide (DMSO) is frequently used as a co-solvent. Time-de-

Table 1. Crystal data and structure refinement parameters for complexes I and II

Crystal data	$[Ni(MPAFA)_3](BF_4)_2$ (I)	[Co(MPAFA) ₃](BF ₄) ₂ (II)	
Empirical formula	C ₃₀ H ₃₃ B ₂ F ₈ N ₉ NiO ₃	C ₃₀ H ₃₃ B ₂ F ₈ N ₉ CoO ₃	
Formula weight	799.96	800.20	
Temperature/K	173	173	
Crystal system	Monoclinic	Monoclinic	
Space group	P2 ₁ /c	P2 ₁ /c	
a/Å	13.0905(5)	13.1847(4)	
b/Å	15.1604(5)	15.1337(4)	
c/Å	18.2845(7)	18.4095(6)	
α/°	90.0000	90.0000	
β/°	105.003(4)	105.613(4)	
ν/°	90.0000	90.0000	
Volume/Å ³	3505.0(2)	3537.77(19)	
Z	4	4	
$\rho_{\rm calc} { m g/cm^3}$	1.516	1.502	
μ/mm^1	0.643	0.574	
F(000)	1640.0	1636.0	
Reflections collected	44820	45274	
Independent reflections (R_{int})	8150 (0.0658)	8179 (0.0495)	
Data/restraints/parameters	8150/206/523	8179/181/523	
Goodness-of-fit on F ²	1.034	1.028	
R_1 , wR_2 [I \geq = 2σ (I)]	0.0502, 0.1027	0.0473, 0.1033	
R_1 , wR_2 [all data]	0.0919, 0.1146	0.0877, 0.1159	
Largest diff. peak/hole / e Å ⁻³	0.52/-0.39	0.47/-0.30	

Table 2. Selected bond lengths (Å) and bond angles (°) of I, II and [Ni(MPAFA)₃](ClO₄)₂

	I		II		[Ni(MPAFA) ₃](ClO ₄) ₂ ⁵⁵	
	Bond length (Å)			Bond length (Å)	- ,	Bond length (Å)
Ni1-N2	2.077(2)	Co1-N2		2.0919(19)	Ni1-N2	2.0825(18)
Ni1-N7	2.120(2)	Co1-N7		2.161(2)	Ni1-N7	2.1262(17)
Ni1-N21	2.105(2)	Co1-N21		2.1631(18)	Ni1-N21	2.1120(18)
Ni1-N16	2.062(2)	Co1-N16		2.117(2)	Ni1-N16	2.0552(18)
Ni1-N30	2.053(2)	Co1-N30		2.0999(19)	Ni1-N30	2.0638(18)
Ni1-N35	2.112(2)	Co1-N35		2.1534(19)	Ni1-N35	2.1127(17)
	Bond angle (°)			Bond angle (°)		Bond angle (°)
N2-Ni1-N7	77.95(8)	N2-Co1-N7		76.46(7)	N2-Ni1-N7	77.83(7)
N7-Ni1-N21	167.04(8)	N7-Co1-N21		98.32(7)	N7-Ni1-N21	97.10(7)
N21-Ni1-N16	77.85(8)	N21-Co1-N16		76.89(7)	N21-Ni1-N16	77.84(7)
N16-Ni1-N35	97.32(8)	N16-Co1-N35		95.13(7)	N16-Ni1-N35	99.46(7)
N35-Ni1-N2	171.50(8)	N35-Co1-N2		101.37(7)	N35-Ni1-N2	93.53(7)
N30-Ni1-N7	91.63(8)	N30-Co1-N7		98.25(8)	N30-Ni1-N7	91.80(7)
N30-Ni1-N35	78.00(8)	N30-Co1-N35		76.70(7)	N30-Ni1-N35	77.90(7)
N30-Ni1-N21	99.32(8)	N30-Co1-N21		91.47(7)	N30-Ni1-N21	96.95(7)
N2-Ni1-N21	94.02(8)	N2-Co1-N21		91.10(7)	N2-Ni1-N21	171.87(7)
N16-Ni1-N30	174.50(8)	N16-Co1-N30		89.35(8)	N16-Ni1-N30	174.13(7)
N35-Ni1-N7	96.71(8)	N35-Co1-N7		91.00(7)	N35-Ni1-N7	166.70(7)
N2-Ni1-N16	89.52(8)	N2-Co1-N16		96.07(8)	N2-Ni1-N16	95.80(7)
N16-Ni1-N7	91.78(8)	N16-Co1-N7		171.17(7)	N16-Ni1-N7	91.54(7)
N35-Ni1-N21	92.36(8)	N35-Co1-N21		165.93(7)	N35-Ni1-N21	92.54(7)
N30-Ni1-N2	95.41(8)	N30-Co1-N2		174.41(8)	N30-Ni1-N2	89.62(7)

pendent UV-Vis spectroscopy was used to determine the stability of the Ni(II) and Co(II) complexes at room temperature in DMSO and DMSO/Tris-HCl buffer (1:1

V/V). The complexes were dissolved in DMSO or DMSO/Tris-HCl buffer (1:1 V/V) at a concentration of 10^{-5} M, over a period of 48 hours, and the stability of I and II was

D-H···A	D-H/(Å)	HA/(Å)	DA/(Å)	<d-h···a (°)<="" th=""><th>Symmetry</th></d-h···a>	Symmetry
			I		
N1-H1···F3 ¹	0.921(17)	2.15(2)	2.932(3)	142(2)	$1 - x$, $\frac{1}{2} + y$, $\frac{1}{2} - z$
N15-H15F1	0.930(18)	2.06(2)	2.847(3)	141(3)	•
N15-H15F3	0.930(18)	2.48(2)	3.313(4)	148(3)	
N29-H29F5	0.937(17)	1.831(18)	2.762(3)	172(3)	
			II		
N1-H1F5	0.924(17)	1.852(18)	2.760(3)	167(2)	
N15-H15··· F4 ¹	0.913(17)	2.14(2)	2.889(3)	139(3)	$1 - x$, $\frac{1}{2} + y$, $\frac{3}{2} - z$
N29-H29F1	0.943(17)	2.01(2)	2.830(3)	144(3)	,
N29-H29F4	0.943(17)	2.58(2)	3.416(5)	147(2)	

Table 3. Hydrogen bonding dimensions of complexes I and II

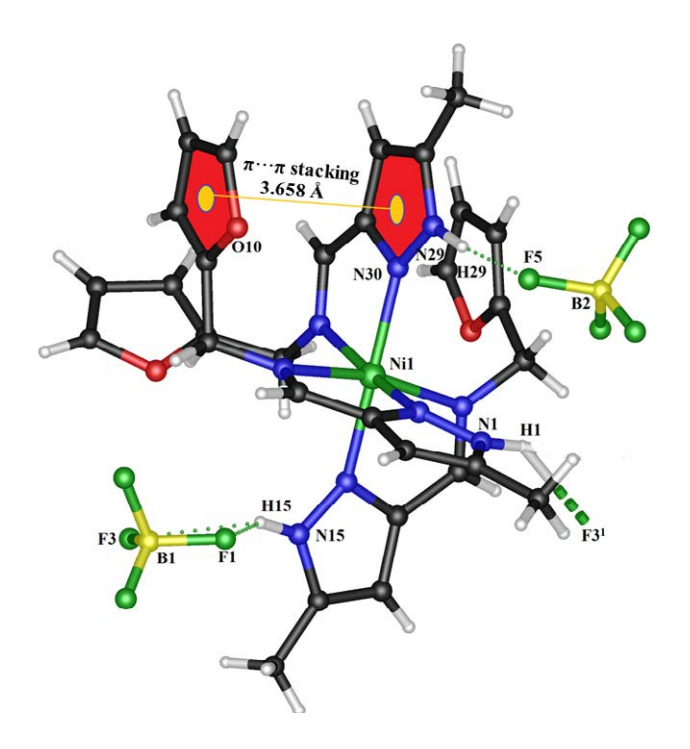


Figure 4. Hydrogen bonding and $\pi...\pi$ stacking diagram of complex I.

confirmed by their UV-Vis spectral patterns (which were almost same, no significant changes were noticed, Figures S7 and S8).

3. 6. 2. Absorption Spectral Studies

The UV-Vis spectroscopic technique was used to evaluate the binding characteristics of **I** and **II** with CT-DNA. Observing the changes in the absorption spectra of the complexes upon addition of increasing amounts of DNA is one of the most extensively utilised approaches for analysing their binding abilities. Figures 6 and 7 depicted the absorption spectra of **I** and **II** at fixed concentrations and in the presence of increasing concentrations of CT-DNA, respectively. As increasing amounts of DNA were

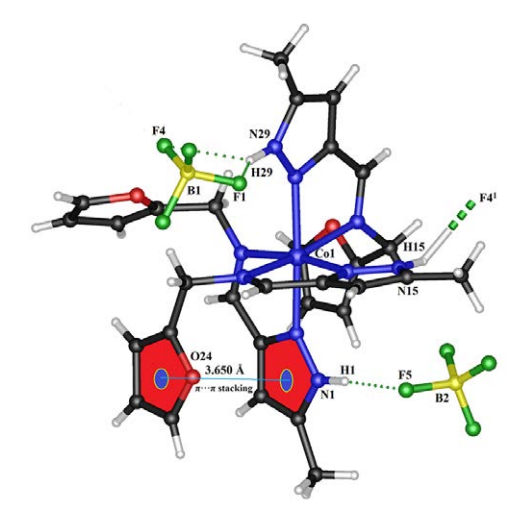


Figure 5. Hydrogen bonding and $\pi...\pi$ stacking diagram of complex II.

added, the UV-Vis spectra of I were found to exhibit a hypochromic effect, while the same for II demonstrated a hyperchromic effect of the charge transfer region. Hence, a 2 nm red-shift of **I** absorption maximum (λ_{max} **I** = 240 nm) when CT-DNA bound I ($\lambda_{max} = 242$ nm; Figure 6) and a 4 nm blue-shift of II absorption maximum (λ_{max} II = 244 nm) when CT-DNA bound II ($\lambda_{max} = 240$ nm; Figure 7) were observed. These changes highlighted the uniqueness of the complexes that interacted with CT-DNA via non-covalent and / or covalent interactions.⁷⁰ The hyperchromism or hypochromism, as well as significant red or blue shifts for I and II, indicated that DNA was interacting with the complexes in solution. As complexes I and II exhibited hypochromism and hyperchromism effects, respectively, it might be concluded that I and II were bound with CT-DNA via the partial intercalative mode⁷¹ and the groove binding mode,⁷² respectively. By the help of eqn. (1), one can calculate the intrinsic binding constant (K_b) values from the plots of [DNA] versus [DNA] / $(\varepsilon_a - \varepsilon_f)$ for I and II in order to understand the strength of the binding between DNA and the complexes. The ε_b , ε_f and ε_a were

the metal complex extinction coefficient in fully bounded form, the extinction coefficient of the free metal complex and the ratio of absorbance/[complex], respectively; [DNA] indicated the concentration of DNA.

$$[DNA] / (\varepsilon_a - \varepsilon_f) = [DNA] / (\varepsilon_b - \varepsilon_f) + 1/Kb (\varepsilon_b - \varepsilon_f)$$
 (1)

The values of $K_{\rm b}$ were observed to be (1.828 \pm 0.349) \times 10⁴ M⁻¹ and (2.105 \pm 0.399) \times 10⁴ M⁻¹ for **I** and **II**, respectively, which were calculated from the slope to intercept ratios in the plots of [DNA] vs. [DNA]/($\epsilon_{\rm a}$ - $\epsilon_{\rm f}$).

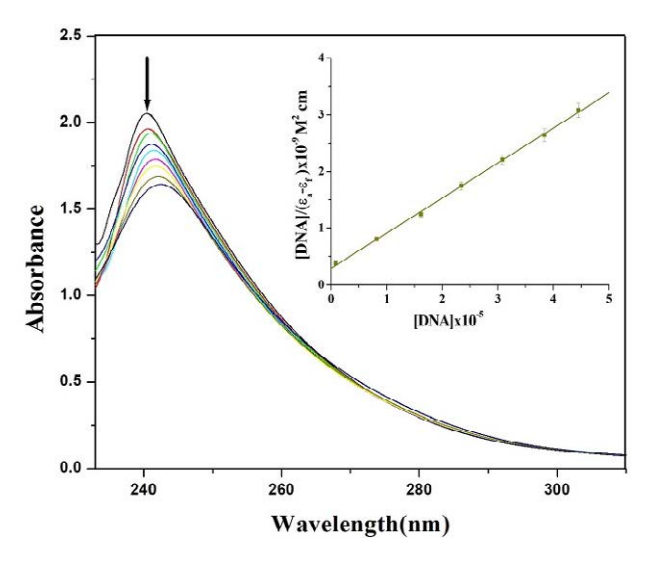


Figure 6. UV-Vis titration spectra of complex **I** $(1.25 \times 10^{-4} \text{ M})$ in 30 mM Tris-HCl buffer at pH 7.5 upon addition of CT-DNA. Inset: [DNA]/ $(\epsilon_n - \epsilon_f)$ vs. [DNA] plot.

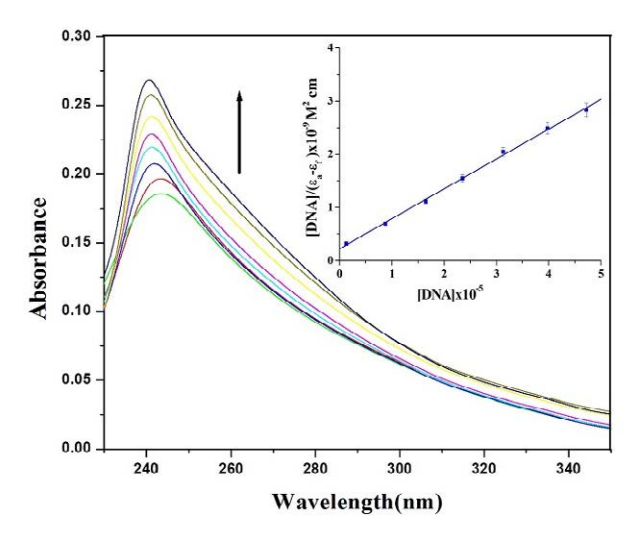


Figure 7. UV-Vis titration spectra of complex II $(1.25 \times 10^{-4} \text{ M})$ in 30 mM Tris-HCl buffer at pH 7.5 upon addition of CT-DNA. Inset: [DNA]/ $(\epsilon_a - \epsilon_f)$ vs. [DNA] plot.

3. 6. 3. Fluorescence Spectral Studies

To achieve a better understanding of DNA binding activities, the competitive binding of ethidium bromide

(EB) vs. the synthesised metal complexes (I and II) with CT-DNA using fluorescence spectroscopy was studied. There was no emission from unbound EB because solvent molecules quenched its fluorescence. In presence of DNA, significant fluorescence was detected as a result of the interaction with DNA base pairs. Upon raising the concentration of the complexes, the emission intensity of EB was found to reduce. Figures S9 and S10 showed the emission spectra of the DNA-EB adducts in absence and in presence of I and II, respectively. As the concentration of the metal complexes increases, a considerable decrease in emission intensity was observed at 591 and 590 nm for I and II, respectively. Generally, some small molecules will be bound and others will remain unbound when they interact independently with a set of equivalent macromolecule sites. The Scatchard equation illustrated the equilibrium between the bounded and unbounded molecules⁷³: log $[(I_0 - I)/I] = \log[K] + n \log[Q]$; where n and K denoted the binding sites and the number of binding constants, respectively, I and I_0 were the fluorescence intensities in the presence and absence of the quencher, respectively. Thus, the values of the binding constants were found to be (3.298 ± 0.177) $\times 10^{3}$ M⁻¹ and (3.742 ± 0.113) $\times 10^{3}$ M⁻¹ for I and II, respectively, from the plots of log[Q] vs. $log[(I_0 -$ I)/I, which were shown in Figures 8 and 9, respectively. As per the result, the binding constant of II was larger than I, which agreed well with the results obtained from UV-Vis spectral studies.

By analysing the values of the binding constants obtained from the UV-Vis titration and fluorescence studies, the affinities for binding of complexes I and II could be determined. It was proposed that I and II bound differently with CT-DNA under the experimental binding conditions. The presence of different metal ions might be the cause of the observed differential in binding affinities and binding modes between the Ni(II) and Co(II) complexes. According to the study, it might be inferred that, in solution, I interacted with CT-DNA via partial intercalation mode,

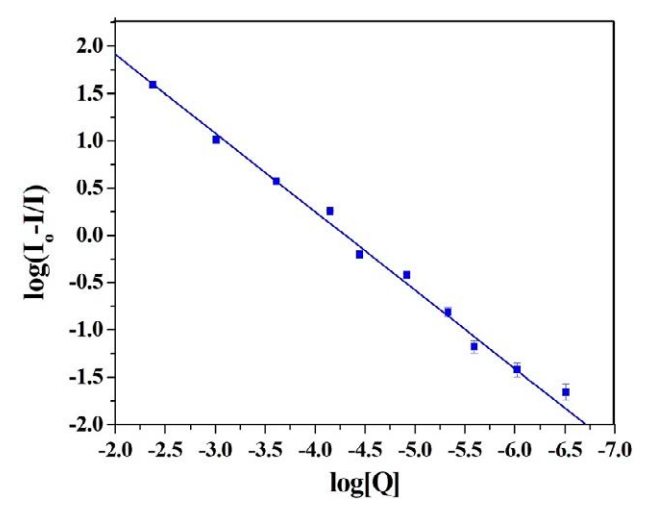


Figure 8. Scatchard plot of log $[(I_0 - I)/I]$ vs. log [Q] for complex **I.**

while II did the same via groove binding or electrostatic mode.

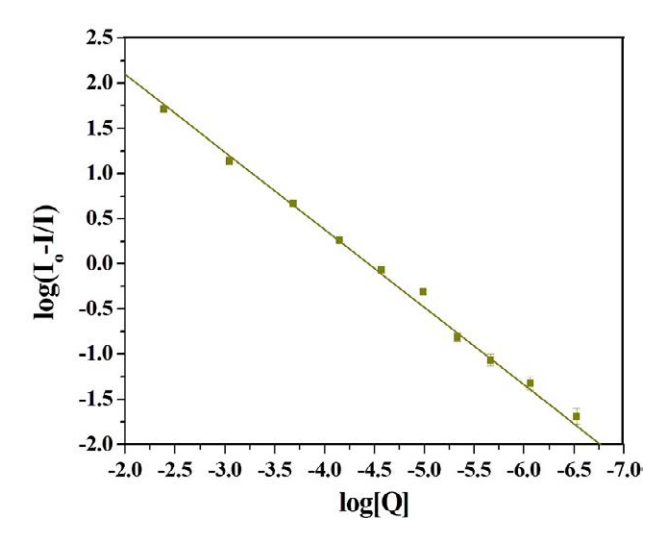


Figure 9. Scatchard plot of $\log [(I_0 - I)/I]$ *vs.* $\log [Q]$ for complex **II.**

3. 6. 4. Viscosity Measurement

Since viscosity of DNA is sensitive to changes in DNA length, measurement of viscosity in solution can be used to evaluate the DNA binding mode of the complexes.⁶³ In general, conventional intercalation causes the base pairs of DNA to split in order to accommodate the constrained metal complexes, resulting in an increase in DNA viscosity.⁷⁴ However, the groove binding mode or partial intercalative mode can leave the viscosity unchanged or even decrease it, indicating that the DNA helix will shorten its effective length.⁷⁵ Therefore, the viscosity may increase for the intercalation mode while remaining same or even decreasing for the groove binding mode. Hence,

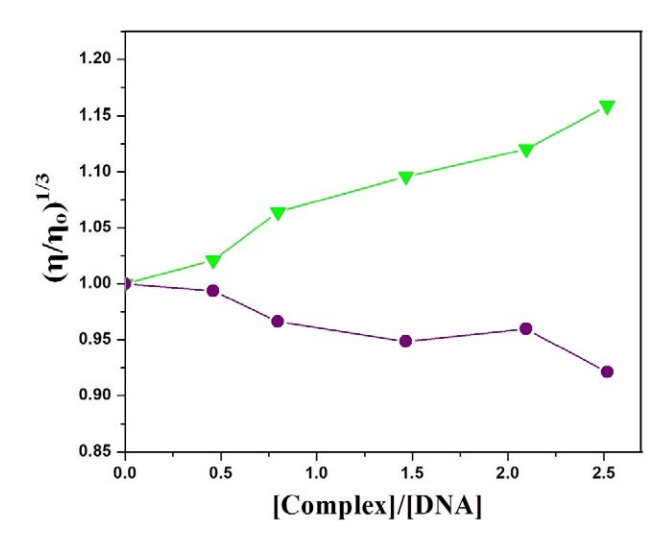


Figure 10. The relative viscosity profile of DNA $(25 \times 10^{-5} \text{ M})$ in 30 mM Tris-HCl buffer upon increasing concentrations of complexes **I** (\triangle) and **II** (\bigcirc) at 25 °C.

the relative specific viscosities, $\{(\eta/\eta_0)^{1/3}\}$, versus the binding ratios, $\{[\text{complex}]/[\text{DNA}]\}$, were plotted, where η and η_0 were the specific viscosities of DNA in presence and in absence of the complex species, respectively (Figure 10). Furthermore, Figure 10 showed that the experiments using UV-Vis titration and fluorescence displacement based on ethidium bromide supported the results obtained from viscosity measurements.

3. 7. Photocatalytic Activities

Methylene blue (MB) was selected as a model pollutant to investigate the photocatalytic activity of the ligand (L) and the metal complexes (I and II), because of its toxicity, carcinogenicity, non-biodegradability and widespread applications in the textile and paper industries. According to the experiment, the photocatalytic studies were carried out under UV-Vis light irradiation. First, the stability of each of the compounds was evaluated using a blank experiment employing only UV light and no MB. The compounds did not degrade after 140 minutes of intense irradiation, according to FTIR (Figure S11) and UV-Vis (Figure S12) spectral measurements. The characteristic absorption peaks of MB in aqueous solutions were found to weaken drastically as the irradiation period got prolonged (Figures 11, 12 and 13); after 140 minutes of UV irradiation, the photocatalytic degradation efficiencies of MB were found to increase in the presence of the compounds, reaching 64.2% for L, 90.5% for I, and 89.6% for II. Only 14.8% of the MB was found to degrade within 140 minutes in the blank experiment, demonstrating the extremely low self-photosensitivity of the MB solution without a catalyst ($K_4 = 0.00106 \text{ min}^{-1}$) (Figure 14). It was clear that the ligand and its complexes exhibited strong photocatalytic activity for the degradation of MB. The ligand (L) in this instance was less active than the associated metal complexes (I and II). These experimental results implied that MB photodegradation effectiveness might be significantly influenced by the type of metal ions present in the complexes. 76 The following pseudo-first-order kinetic equation (1) was used to analyze the photocatalytic degradation of MB in aqueous solution.

$$-\ln(A/A_0) = Kt \tag{1}$$

By plotting $-\ln(A/A_0)$ vs. t (A = maximum absorbance of MB at variable irradiation time 't', A_0 = maximum absorbance of MB at initial time of irradiation), three straight lines passing from the origin with the slopes of 0.00472 (K_1 = 0.00472 min⁻¹), 0.01149 (K_2 = 0.01149 min⁻¹) and 0.01036 (K_3 = 0.01036 min⁻¹) for **L**, **I** and **II**, respectively, were obtained (Figure 14). Hence the outcome indicated that the compounds **L**, **I**, and **II** could behave as UV-responsive photocatalysts and might be employed to degrade organic dye pollutants, with an appreciable degradation efficiency (\sim 90% for the metal complexes).

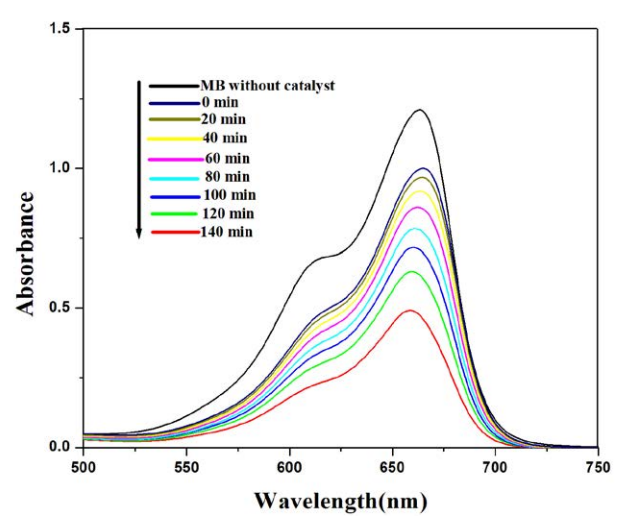


Figure 11. The absorption spectra of the MB solutions during the degradation reaction under UV light irradiation in the presence of ligand **L**.

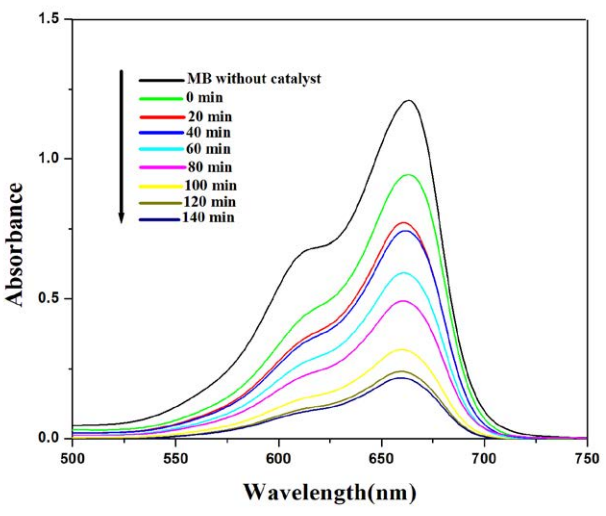


Figure 12. The absorption spectra of the MB solutions during the degradation reaction under UV light irradiation in the presence of **I.**

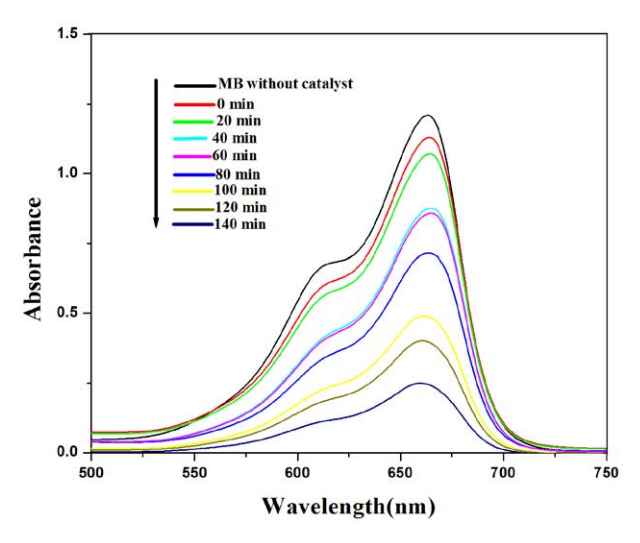


Figure 13. The absorption spectra of the MB solutions during the degradation reaction under UV light irradiation in the presence of II.

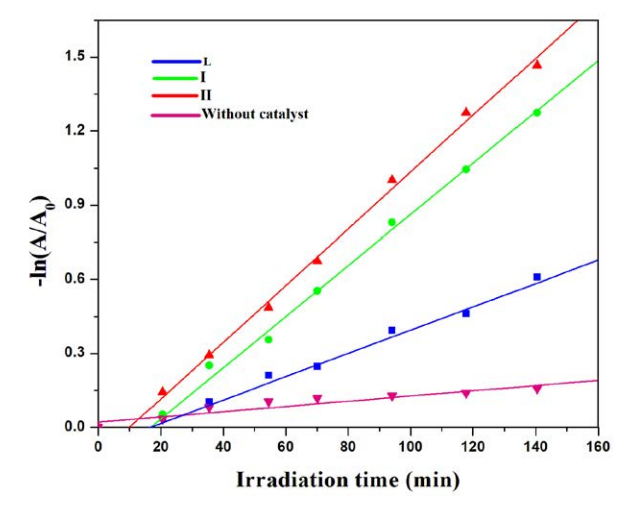


Figure 14. The pseudo-first-order plot of MB solution under UV light irradiation with the use of **L**, **I** and **II** and no crystal in the same conditions (**L**: $K_1 = 0.00472 \text{ min}^{-1}$; **I**: $K_2 = 0.01149 \text{ min}^{-1}$; **II**: $K_3 = 0.01036 \text{ min}^{-1}$; without catalyst: $K_4 = 0.00106 \text{ min}^{-1}$). The dots and the line represented the experimental data and the fitted line, respectively.

3. 7. 1. Possible Photocatalytic Mechanism

The following explanations could be given for a probable pathway of degradation of dyes.^{77–80} In the first step of irradiation of the compounds, the electrons (e⁻) to be excited from the highest occupied molecular orbital (HOMO) and transition to the lowest unoccupied molecular orbital (LUMO) as:

Compound +
$$hv(UV) \rightarrow Compound(e_{LUMO}^- + h_{HOMO}^+)$$

In the second step e^- in LUMO might combine with dissolved oxygen (O_2) and then produce $O_2^{\bullet-}$ radical-anion, which reacted with water to produce OH^{\bullet} radical as:

$$O_2 + e^-_{LUMO} \longrightarrow O_2^{\bullet -}$$

$$O_2^{\bullet -} + H_2O \longrightarrow OH^{\bullet} + H_2O_2$$

HOMO was in metastable states at the same time and needed e^- to return to steady states. To create OH*, the h+ in HOMO trapped the e^- in H₂O as:

$$H_2O + h^+_{HOMO} \longrightarrow OH^*$$

Then highly active OH active OH radical oxidised MB to CO₂ as:

$$MB+OH$$
 \longrightarrow $CO_2 + H_2O + other products$

4. Conclusions

Here, the synthesis, characterization, X-ray crystal structures, DNA binding ability and photocatalytic ac-

tivity of two Ni(II) and Co(II) complexes of a Schiff base ligand, N-(furan-2-ylmethyl)-1-(5-methyl-1H-pyrazol-3yl)methanimine, (MPAFA) have been discussed. Both the metal ions form (1:3) complexes with the 'NN' bidentate ligand and in the complex species, the metal centres assume a distorted octahedral geometry with a NiN6 and CoN6 donor sets, for I and II, respectively. The complexes display non-covalent interactions like hydrogen bonding, and $\pi...\pi$ stacking (between the centroid of pyrazole and furan rings). Both I and II exhibit fluorescence activity and II has been found to be more luminescent. DNA interaction studies reveal that both the metal complexes interact with the CT-DNA and I binds with CT-DNA in a partial intercalative manner, while II binds via groove-like mode. The ligand and the metal complexes show significant catalytic activities for photodegradation of MB under UV light irradiation. It has been found that I and II displayed higher photocatalytic efficiency in degrading MB than the free ligand L.

Acknowledgement

One of us (Suman Mandal) is thankful to the University of Kalyani for providing financial support in the form of University Research Scholarship. N.C. Saha is thankful to the University of Kalyani for financial assistance received in the form of Personal Research Grant. The instrumental facilities received from the DST-FIST (Level-2; SR/FST/CSII/2019/96) program in the Department of Chemistry, University of Kalyani are thankfully acknowledged.

Supplementary Data

CCDC deposition numbers 2241527 and 2152086 contain the supplementary crystallographic data for complexes I and II, respectively. These data can be obtained free of charge via http://www.ccdc.cam.ac.uk/conts/retrieving.html, or from the Cambridge Crystallographic Data Centre, 12 Union Road, Cambridge CB2 1EZ, UK; fax: (+44) 1223-336-033; or e-mail: deposit@ccdc.cam. ac.uk. Figures S1-S12 and Table S1 are available as supporting information file.

5. References

- M. Ikram, S. Rehman, I. Feroz, R. Khan, M. O. Sinnokrot, F. Subhan, M. Naeem, C. Schulzke, *J. Mol. Struct.* 2023, 1278, 134960. DOI:10.1016/j.molstruc.2023.134960
- F. Purtas, K. Sayin, G. Ceyhan, M. Kose, M. Kurtoglu, J. Mol. Struct. 2017, 1137, 461–475.
 - DOI:10.1016/j.molstruc.2017.02.065
- M. Rocha, A. D. Santo, G. A. Echeverría, O. E. Piro, F. D. Cukiernik, S. E. Ulic, D. M. Gil, *J. Mol. Struct.* 2017, 1133, 24–36. DOI:10.1016/j.molstruc.2016.11.071
- 4. X. C. Shi, H. B. Fang, Y. Guo, H. Yuan, Z. J. Guo, X. Y. Wang,

- J. Inorg. Biochem. **2019**, 190, 38–44.
- **DOI:**10.1016/j.jinorgbio.2018.10.003
- T. R. Lakshman, J. Deb, I. Ghosh, S. Sarkar, T. K. Paine, *Inorg. Chim. Acta* 2019, 486, 663–668.
 - DOI:10.1016/j.ica.2018.11.025
- C. M. da Silva, D. L. da Silva, L. V. Modolo, R. B. Alves, M. A. de Resende, C. V. B. Martins, Â. de Fátima, *J. Adv. Res.* 2011, 2, 1–8. DOI:10.1016/j.jare.2010.05.004
- P. Przybylski, A. Huczynski, K. Pyta, B. Brzezinski, F. Bartl, *Curr. Org. Chem.* 2009, 13, 124–148.
 - **DOI:**10.2174/138527209787193774
- 8. P. Ghorai, R. Saha, S. Bhuiya, S. Das, P. Brandao, D. Ghosh, T. Bhaumik, P. Bandyopadhyay, D. Chattopadhyay, A. Saha, *Polyhedron* **2018**, *141*, 153–163.
 - DOI:10.1016/j.poly.2017.11.041
- A. Singh, S. K. Maiti, H. P. Gogoi, P. Barman, *Polyhedron* 2023, 230, 116244. DOI:10.1016/j.poly.2022.116244
- H. Kargar, R. Behjatmanesh-Ardakani, V. Torabi, M. Kashani,
 Z. Chavoshpour-Natanzi, Z. Kazemi, V. Mirkhani, A. Sahraei,
 M. N. Tahir, M. Ashfa, K. S. Munawar, *Polyhedron* 2021, 195,
 114988. DOI:10.1016/j.poly.2020.114988
- E. Colacio-Rodriguez, J. D. Lopez-Gonzalez, J. M. Salas-Peregrin, *Can. J. Chem.* 1983, *61*, 2506–2508.
 DOI:10.1139/v83-432
- V. Razakantoanina, N. K. P. Phung, G. Jaureguiberry, *Parasitol. Res.* 2000, 86, 665–668. DOI:10.1007/PL00008549
- R. Baumgrass, M. Weiwad, F. Erdmann, J. O. Liu, D. Wunderlich, S. Grabley, G. Fischer, *J. Biol. Chem.* **2001**, *276*, 47914–47921. **DOI**:10.1074/jbc.M103273200
- M. Shabbir, Z. Akhter, I. Ahmad, S. Ahmed, H. Ismail, B. Mirza, V. McKee, M. Bolte, *J. Mol. Struct.* **2016**, *1116*, 84–92.
 DOI:10.1016/j.molstruc.2016.03.008
- M. Tolomeo, D. Simoni, Curr. Med. Chem. 2002, 2, 387–401.
 DOI:10.2174/1568011024606361
- J. H. Goldie, Cancer Metast. Rev. 2001, 20, 63–68.
 DOI:10.1023/A:1013164609041
- V. V. Arion, E. Reisner, M. Fremuth, M. A. Jakupec, B. K. Keppler, V. Y. Kukushkin, A. J. L. Pombeiro, *Inorg. Chem.* 2003, 42, 6024–6031. DOI:10.1021/ic034605i
- F. Ahmadi, A. A. Alizadeh, N. Shahabadi, M. Rahimi-Nasrabadi, *Spectrochim. Acta, Part A* 2011, 79, 1466–1474.
 DOI:10.1016/j.saa.2011.05.002
- G. Barone, A. Terenzi, A. Lauria, A. M. Almerico, J. M. Leal,
 N. Busto, B. García, *Coord. Chem. Rev.* 2013, 257, 2848–2862.
 DOI:10.1016/j.ccr.2013.02.023
- A. Sigel, H. Sigel, R. K. O. Sigel, Nickel and Its Surprising Impact in Nature, John Wiley & Sons Ltd, New York, 2007.
 DOI:10.1002/9780470028131
- 21. J. J. R. F. da Silva, R. J. P. Williams, The Biological Chemistry of the Elements, Oxford University Press, Oxford, **2001**.
- 22. R. K. Andrews, R. L. Blakeley, B. Zerner, H. Sigel, A. Sigel, Nickel in biology, in: Metal Ions in Biological Systems, Marcel Dekker Inc, New York, **1988**, 168–171.
- 23. B. Claudio, G. A. Colditz, Nickel compound, in: The SAGE Encyclopedia of Cancer and Society, SAGE Publications, Inc., 2015, 828–831.

- 24. S. Perontsis, A. G. Hatzidimitriou, A. N. Papadopoulos, G. Psomas, *J. Inorg. Biochem.* **2016**, *162*, 9–21. **DOI:**10.1016/j.jinorgbio.2016.06.003
- R. Kurtaran, L. T. Yildirim, A. D. Azaz, H. Namli, O. Atakol, J. Inorg. Biochem. 2005, 99, 1937–1944.
 DOI:10.1016/j.jinorgbio.2005.05.016
- Z. Afrasiabi, E. Sinn, W. Lin, Y. Ma, C. Campana, S. Padhye, *J. Inorg. Biochem.* 2005, 99, 1526–1531.
 DOI:10.1016/j.jinorgbio.2005.04.012
- B. B. Xu, P. Shi, Q. Y. Guan, X. Shi, G. L. Zhao, J. Coord. Chem.
 2013, 66, 2605–2614. DOI:10.1080/00958972.2013.811497
- F. Bisceglie, S. Pinelli, R. Alinovi, M. Goldoni, A. Mutti, A. Camerini, L. Piola, P. Tarasconi, G. Pelosi, *J. Inorg. Biochem.* 2014, 140, 111–125. DOI:10.1016/j.jinorgbio.2014.07.014
- 29. A. Sigel, H. Sigel, R. K. O. Sigel (Eds.), Interrelation between Essential Metal Ions and Human Diseases in: Metal Ions in Life Sciences, Spinger, Dordrecht, **2013**, *13*, 295–320. **DOI:**10.1007/978-94-007-7500-8 **ISBN:** 978-94-007-7500-8 (eBook)
- H. R. Zhang, K. B. Huang, Z. F. Chen, Y. C. Liu, Y. N. Liu, T. Meng, Q. P. Qin, B. Q. Zou, H. Liang, *MedChemComm* 2016, 7, 806–812. DOI:10.1039/C6MD00073H
- S. Adewuyi, K. T. Kareem, A. O. Atayese, S. A. Amolegbe, C. A. Akinremi, *Int. J. Biol. Macromol.* 2011, 48, 301–303.
 DOI:10.1016/j.ijbiomac.2010.12.004
- 32. M. Patel, M. Chhasatia, B. Bhatt, *Med. Chem. Res.* **2011**, *20*, 220–230. **DOI:**10.1007/s00044-010-9310-9
- P. Sathyadevi, P. Krishnamoorthy, M. Alagesan, K. Thanigaimani, P. Thomas Muthiah, N. Dharmaraj, *Polyhedron*, 2012, 31, 294–306. DOI:10.1016/j.poly.2011.09.021
- 34. S. Shreaz, R. A. Sheikh, R. Bhatia, K. Neelofar, S. Imran, A. A. Hashmi, N. Manzoor, S. F. Basir, L. A. Khan, *Biometals* **2011**, 24, 923–933. **DOI:**10.1007/s10534-011-9447-0
- 35. M. R. Hoffmann, S. T. Martin, W. Choi, D. W. Bahnemann, *Chem. Rev.* **1995**, 95, 69–96. **DOI:**10.1021/cr00033a004
- P. C. Vandevivere, R. Bianchi, W. J. Verstraete, *Chem. Technol. Biotechnol.* 1998, 72, 289–302.
 DOI:10.1002/(SICI)1097-4660(199808)72:4<289::AID-

JCTB905>3.3.CO;2-R

- C. -C. Wang, J. -R. Li, X. -L. Lv, Y. -Q. Zhang, G. Guo, *Energy Environ*. Sci. 2014, 7, 2831–2867. DOI:10.1039/C4EE01299B
- A. Kuila, N. A. Surib, N. S. Mishra, A. Nawaz, K. H. Leong,
 L. C. Sim, P. Saravanan, S. Ibrahim, *ChemistrySelect* 2017, 2,
 6163–6177. DOI:10.1002/slct.201700998
- M. Li, L. Liu, L. Zhang, X. Lv, J. Ding, H. Hou, Y. Fan, CrystEng-Comm. 2014, 16, 6408–6416. DOI:10.1039/C4CE00093E
- 40. P. Mahata, G. Madras, S. Natarajan, *J. Phys. Chem. B***2006**, *110*, 13759–13768. **DOI**:10.1021/jp0622381
- 41. L. Liu, J. Ding, C. Huang, M. Li, H. Hou, Y. Fan, *Cryst. Growth Des.* **2014**, *14*, 3035–3043. **DOI**:10.1021/cg500295r
- J.-C. Jin, J. Wu, W.-C. Liu, A.-Q. Ma, J.-Q. Liu, A. Singh, A. Kumar, *New J. Chem.* 2018, 42, 2767–2775.
 DOI:10.1039/C7NJ04355D
- 43. W. Meng, Z. Xu, J. Ding, D. Wu, X. Han, H. Hou, Y. Fan, *Cryst. Growth Des.* **2014**, *14*, 730–738. **DOI:**10.1021/cg401601d
- 44. L. L. Wen, L. Zhou, B. G. Zhang, X. G. Meng, H. Qua, D. F. Li,

- *J. Mater. Chem.* **2012**, 22, 22603–22609. **DOI:**10.1039/c2jm34349e
- 45. X. Zhuang, Y. Wan, C. Feng, Y. Shen, D. Zhao, *Chem. Mater.* **2009**, *21*, 706–716. **DOI**:10.1021/cm8028577
- 46. Y. Lee, S. G. Zimmermann, A. T. Kieu, U. V. Gunten, *Environ*. *Sci. Technol.* **2009**, *43*, 3831–3838. **DOI:**10.1021/es803588k
- 47. J. Tang, Y. Liu, H. Li, Z. Tan, D. Li, *Chem. Commun.* **2013**, 49, 5498–5500. **DOI:**10.1039/c3cc41090k
- 48. Z. Xu, X. Mao, P. Zhang, H. Li, Y. Wang, M. Liu, L. Jia, J. Mol. Struct. 2017, 1128, 665–673.
 DOI:10.1016/j.molstruc.2016.09.041
- 49. G. Guan, E. Ye, M. You, Z. Li. *Small* **2020**, *16*, 1907087. **DOI:**10.1002/smll.201907087
- Z. Youssef, L. Colombeau, N. Yesmurzayeva, F. Baros, R. Vanderesse, T. Hamieh, J. Toufaily, C. Frochot, T. Roques-Carmes. *Dyes Pigm.* 2018, 159, 49–71.
 DOI:10.1016/j.dyepig.2018.06.002
- 51. M. Dai, H.-X. Li, J.-P. Lang, *CrystEngComm*. **2015**, *17*, 4741–4753. **DOI:**10.1039/C5CE00619H
- 52. B. R. Kirthan, M. C. Prabhakara, H. S. Bhojyanaik, P. H. Amith Nayak, R. Viswanath, H. B. Teja, Ereshanaik, *Inorg. Chem. Commun.* 2022, 135, 109109.
 DOI:10.1016/j.inoche.2021.109109
- R. S. Joseyphus, R. Reshma, D. Arish, V. Elumalai, *Results Chem.* 2022, 4, 100583. DOI:10.1016/j.rechem.2022.100583
- 54. X.-S. Hong, D. Huo, W.-J. Jiang, W.-J. Long, Ji-D. Leng, L. Tong, Z.-Q. Liu, *ChemElectroChem*, **2020**, 7, 4956–4962. **DOI:**10.1002/celc.202001461
- S. Mandal, M. Sarkar, S. Denrah, A. Bagchi, A. Biswas, D. B. Cordes, A. M. Z. Slawin, N. C. Saha, *J. Mol. Struct.* **2023**, 1287, 135648. **DOI**:10.1016/j.molstruc.2023.135648
- 56. CrystalClear-SM Expert v2.1. Rigaku Americas, The Woodlands, Texas, USA, and Rigaku Corporation, Tokyo, Japan, 2015
- CrysAlisProv1.171.38.46. Rigaku Oxford Diffraction, Rigaku Corporation, Oxford, U.K., 2015
- G. M. Sheldrick, Acta Crystallogr., Sect. A. 2015, 71, 3–8.
 DOI:10.1107/S2053273314026370
- M. C. Burla, R. Caliandro, M. Camalli, B. Carrozzini, G. L. Cascarano, L. De Caro, C. Giacovazzo, G. Polidori, R. Spagna, J. Appl. Crystallogr. 2005, 38, 381–388.
 DOI:10.1107/S002188980403225X
- G. M. Sheldrick, Acta Crystallogr., Sect. C. 2015, 71, 3–8.
 DOI:10.1107/S2053273314026370
- O. V. Dolomanov, L. J. Bourhis, R. J. Gildea, J. A. K. Howard, H. Puschmann, *J. Appl. Crystallogr.* 2009, 42, 339–341.
 DOI:10.1107/S0021889808042726
- 62. D. Sarkar, P. Das, S. Basak, N. Chattopadhyay, *J. Phys. Chem. B* **2008**, *112*, 9243–9249. **DOI:**10.1021/jp801659d
- N. Dutta, A. Majumder, A. Das, A. Chatterjee, M. Bera, *J. Mol. Struct.* 2020, 1206, 127708.
 DOI:10.1016/j.molstruc.2020.127708
- N. C. Saha, S. Mandal, M. Das, N. Khatun, D. Mitra, A. Samanta, A. M. Z. Slawin, R. J. Butcher, R. Saha, *Polyhedron* 2014, 68, 122–130. DOI:10.1016/j.poly.2013.10.016
- 65. V. L. Siji, M. R. Sudarsanakumar, S. Suma, Polyhedron 2010,

- 29, 2035-2040. DOI:10.1016/j.poly.2010.03.011
- S. Konar, A. Jana, S. K. Kar, *Polyhedron* 2011, *30*, 2801–2808.
 DOI:10.1016/j.poly.2011.08.018
- L. J. Farrugia, WinGX and ORTEP for Windows: an update, *J. Appl. Crystallogr.* 2012, 45, 849–854.
 DOI:10.1107/S0021889812029111
- C. Janiak, J. Chem. Soc., Dalton Trans. 2000, 21, 3885–3896.
 DOI:10.1039/b003010o
- Y. Zhao, J. Li, H. Gu, D. Wei, Y.-C. Xu, W. Fu, Z. Yu, Interdiscip. Sci. Comput. Life Sci. 2015, 7, 211–220.
 DOI:10.1007/s12539-015-0263-z
- A. Tarushi, G. Psomas, C. P. Raptopoulou, D. P. Kessissoglou, J. Inorg. Biochem. 2009, 103, 898–905.
 DOI:10.1016/j.jinorgbio.2009.03.007
- 71. A. Majumder, S. Haldar, N. Dutta, A. Das, M. Bera, *ChemistrySelect* **2022**, *7*, 1–15. **DOI**:10.1002/slct.202104319
- J. R. Lakowicz, Fluorescence Quenching: Theory and Applications. Principles of Fluorescence Spectroscopy, Kluwer Academic/Plenum Publishers, New York, 1999, 53–127.
 DOI:10.1007/978-1-4757-3061-6_8

- D. Suh, J. B. Chaires, Bioorg. Med. Chem. 1995, 3, 723–728.
 DOI:10.1016/0968-0896(95)00053-J
- 74. H. Wu, J. Yuan, Y. Bai, H. Wang, G. Pan, J. Kong, J. Photochem. Photobiol. B 2012, 116, 13–21.
 DOI:10.1016/j.jphotobiol.2012.07.005
- A. Chouai, S. E. Wicke, C. Turro, J. Bacsa, K. R. Dunbar, D. Wang, R. P. Thummel, *Inorg. Chem.* 2005, 44, 5996–6003.
 DOI:10.1021/ic0485965
- C. Patricio, H. Yosselin, R. Walter, C. Jonathan, B. Ivan, A. Rodrigo, *Appl. Organomet. Chem.* 2020, e5974.
 DOI:10.1002/aoc.5974
- W. Kang, W. Zhong, C. Li, F. Xia, Y. Wu, O. Prakash, A. Kumar, H. Sakiyama, M. Muddassir, *Polyhedron* **2022**, *228*, 116158. **DOI**:10.1016/j.poly.2022.116158
- 78. M. Pandey, R. Prajapti, P. Shukla, P. Paredi, N. Tsunoji, R. Kumar, S. Shahabuddin, S. Das, M. Bandyopadhyay, *Polyhedron* **2022**, *228*, 116161. **DOI**:10.1016/j.poly.2022.116161
- J. X. Li, Y. F. Li, L. W. Liu, G. H. Cui, *Ultrasonics –Sonochem*.
 2018, 41, 196. DOI:10.1016/j.ultsonch.2017.09.039
- Y. Qu, Y. Yang, G. Dong, *Polyhedron* **2020**, *180*, 114431.
 DOI:10.1016/j.poly.2020.114431

Povzetek

Z ligandom N-(furan-2-ilmetil)-1-(5-metil-1H-pirazol-3-il)metanimin, (MPAFA) (L), ki deluje kot Schiffova baza s pirazolnim obročem, smo sintetizirali dva nova kompleksa niklja(II) in kobalta(II), [Ni(MPAFA)₃]2BF₄ (I) in [Co(M-PAFA)₃]2BF₄ (II). Obe spojini smo karakterizirali z različnimi fizikalno-kemijskimi in spektralnimi metodami. Obe spojini, I in II, imata razmerje M:L = 1:3 in se obnašata kot 1:2 elektrolita. Strukturna analiza na monokristalu kaže za oba kompleksa popačeno oktaedrično zgradbo z N6 donorskimi atomi. Interakcije pri vezavi kompleksa s CT-DNA smo preučevali z UV-Vis in fluorescenčno spektroskopijo. Ligand in kompleksi imajo potencialno fotokatalitsko aktivnost pri razgradnji metilenskega modrila (MB) pod obsevanjem z UV-Vis svetlobo.

